Research Article | Vol. 27, No. 3 | 4 Feb 2019 | OPTICS EXPRESS 2530
Optics EXPRESS

Deep neural networks assisted BOTDA for simultaneous temperature and strain measurement with enhanced accuracy

BIWEI WANG,[1] LIANG WANG,[2,*] NAN GUO,[1] ZHIYONG ZHAO,[1] CHANGYUAN YU,[1,3] AND CHAO LU[1]

[1]*Department of Electronic and Information Engineering, The Hong Kong Polytechnic University, Kowloon, Hong Kong, China*
[2]*Department of Electronic Engineering, The Chinese University of Hong Kong, Shatin, N.T., Hong Kong, China*
[3]*changyuan.yu@polyu.edu.hk*
**lwang@ee.cuhk.edu.hk*

Abstract: Simultaneous temperature and strain measurement with enhanced accuracy by using Deep Neural Networks (DNN) assisted Brillouin optical time domain analyzer (BOTDA) has been demonstrated. After trained by using combined ideal clean and noisy BGSs, the DNN is applied to extract both the temperature and strain directly from the measured double-peak BGS in large-effective-area fiber (LEAF). Both simulated and experimental data under different temperature and strain conditions have been used to verify the reliability of DNN-based simultaneous temperature and strain measurement, and demonstrate its advantages over BOTDA with the conventional equations solving method. Avoiding the small matrix determinant-induced large error, our DNN approach significantly improves the measurement accuracy. For a 24-km LEAF sensing fiber with a spatial resolution of 2m, the root mean square error (RMSE) and standard deviation (SD) of the measured temperature/strain by using DNN are improved to be 4.2°C/134.2με and 2.4°C/66.2με, respectively, which are much lower than the RMSE of 30.1°C/710.2με and SD of 19.4°C/529.1με for the conventional equations solving method. Moreover, the temperature and strain extraction by DNN from 600,000 BGSs along 24-km LEAF requires only 1.6s, which is much shorter than that of 5656.3s by the conventional equations solving method. The enhanced accuracy and fast processing speed make the DNN approach a practical way of achieving simultaneous temperature and strain measurement by the conventional BOTDA system without adding system complexity.

1. Introduction

Brillouin Optical Time Domain Analysis (BOTDA) has attracted a lot of research interest over the past three decades due to its outstanding capability of distributed temperature and strain measurement and hence wide applications in structural health monitoring (SHM) [1,2]. Generally long sensing distance, high spatial resolution, high measurement accuracy, and fast measurement speed are ultimate goals for the development of BOTDA [3–8]. Moreover, to achieve simultaneous temperature and strain measurement is also desirable, although it is difficult to realize it in the conventional BOTDA systems because of the Brillouin scattering induced cross-sensitivity of temperature and strain. To date some solutions have been reported to realize simultaneous temperature and strain measurement [9–22]. Hybrid sensor systems combining Brillouin scattering with either Rayleigh scattering or Raman scattering have been demonstrated to discriminate temperature and strain [9–11]. However, compared with a single BOTDA system, hybrid systems introduce extra system complexity and cost. For a single BOTDA system to discriminate the temperature and strain, one of the methods is to measure the Brillouin frequency shift (BFS) together with Brillouin peak power or

#347556 https://doi.org/10.1364/OE.27.002530
Journal © 2019 Received 4 Oct 2018; revised 30 Dec 2018; accepted 8 Jan 2019; published 28 Jan 2019

Optics EXPRESS

bandwidth or birefringence in a polarization-maintaining fiber (PMF) [12–14], however launching of fiber axis with PMF makes the operation complicated and the power measurement is usually unstable. Another solution is to use multi-core fiber (MCF) [15], where several BFSs obtained from different fiber cores have been used together to measure temperature and strain simultaneously. Moreover, using fibers with multi-peak Brillouin Gain Spectrum (BGS) has been demonstrated to be an elegant solution, such as photonic crystal fiber (PCF) [16], large-effective-area fiber (LEAF) [17–19], dispersion compensating fiber (DCF) [20] and few mode fiber (FMF) [21]. However, because of the small difference of BFS-temperature/strain coefficients between Brillouin peaks, the solving of two BFS equations to recover the temperature and strain produces large errors and hence the obtained temperature and strain resolutions are much larger than single temperature or strain measurement, e.g. 27°C/570με error in 22km long LEAF [18,19]. Besides the poor accuracy, curve fitting process to determine the BFS in the equations solving method usually takes long time, which makes the whole process of temperature and strain extraction time-consuming.

On the other hand, some advanced machine learning techniques have been applied to the conventional single BOTDA system to extract temperature information with better sensing performance compared with curve fitting methods [22–25]. Artificial Neural Network (ANN) has shown higher accuracy and larger tolerance to measurement error in comparison to Lorentzian curve fitting (LCF) and cross-correlation method [22]. Besides the robustness to a wide range of experimental parameters, Support Vector Machine (SVM) has been demonstrated to have a processing speed 100 times faster than Lorentzian curve fitting [23,24]. Compared with ANN, Deep Neural Networks (DNN) with autoencoder can be easily trained to achieve global optimum for temperature extraction in BOTDA [25]. In addition to single temperature measurement, recently we have reported for the first time the preliminary work on the feasibility of using DNN for simultaneous temperature and strain measurement [26], where a single BOTDA system employing the conventional single mode LEAF sensing fiber is adopted and DNN extracts both the temperature and strain directly from the double-peak BGS of LEAF. Unlike the conventional equations solving method [16–21], there is no curve fitting to obtain the BFS of Brillouin peaks and no subsequent procedure of solving two BFS equations. In contrast, the extraction of temperature and strain is regarded as a regression task for DNN, and through training the DNN builds up the relationship between the double-peak BGS and the temperature and strain. Thus compared with the conventional equations solving method, the DNN approach can potentially improve the accuracy of measured temperature and strain, and the whole process of temperature and strain extraction by DNN can be expected to be very fast.

In this paper, we demonstrate the enhanced accuracy and fast processing speed offered by DNN approach, and statistically analyze and compare its performance with the conventional equations solving method through both simulation and experiment. The impact of noise added in the training of DNN is analyzed and the optimal amount of noise needed to improve the DNN tolerance to the noise from measured BGSs is discussed. With a little modification of the experimental setup to make the strain uniform along the LEAF, we have tested a larger range of temperature and strain conditions in this work to verify the reliability of DNN based simultaneous temperature and strain measurement. Our results show that the measured temperature and strain by DNN have much lower root mean square error (RMSE) and standard deviation (SD), which means the measured values are close to the real ones with small fluctuations. Compared with the conventional equations solving method, the DNN based simultaneous temperature and strain measurement improves the measurement accuracy by at least five times, and shortens the processing time by three orders of magnitude.

Optics EXPRESS

2. Principle and simulation

2.1 Principle of using DNN for simultaneous temperature and strain measurement

DNN is an advanced hierarchical neural network which belongs to one type of deep learning models. Its structure is similar to ANN except the training process includes both unsupervised and supervised learning for data size compression which makes the training more efficient. Figure 1 illustrates a general structure of DNN model containing an input layer, several hidden layers and an output layer. Each node represents a neuron and each connecting line represents a synapse with a weight value of w_{ij}. Every hidden layer is formed by an autoencoder including both encoder and decoder. The output of a neuron after input layer can be expressed using the following Eq. (1):

$$y_j = f_j(\sum w_{ij} \cdot x_i - \theta_j) \tag{1}$$

where y_j is the output of the j^{th} neuron in current layer; f_j is the activation function; w_{ij} is the weight of synapse connecting the i^{th} neuron in the previous layer and the j^{th} neuron in the current layer; x_i means the output of the i^{th} neuron in the previous layer; θ_j is a constant bias.

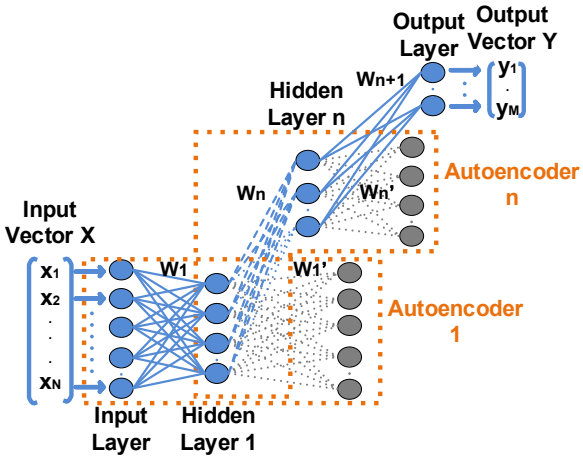

Fig. 1. General structure of DNN with n autoencoder hidden layers. W_n is the weight vector for the n^{th} hidden layer.

Figure 2 shows the principle. The DNN model contains one input layer (I), two hidden layers (H1 and H2) and one output layer (O). In this case, the input vector X (x_1, x_2, …, x_{226}) in Fig. 1 including 226 elements represents the data vector for the double-peak BGS which is injected into the input layer of the DNN. The number of elements in X is equal to the number of scanned frequencies in the BOTDA system. The output vector Y (y_1, y_2) has two elements, corresponding to the temperature and strain. The utilization of DNN contains two main stages: training and testing. Since the BFSs of the double-peak BGS in LEAF are linearly proportional to both the temperature and strain but exhibit different responses, the DNN model can learn the relationship between the double-peak BGS and the temperature/strain after appropriate training process. After training, the designed DNN can be used to extracts the values of temperature and strain directly from the input measured double-peak BGS, which is the so-called testing stage.

Optics EXPRESS

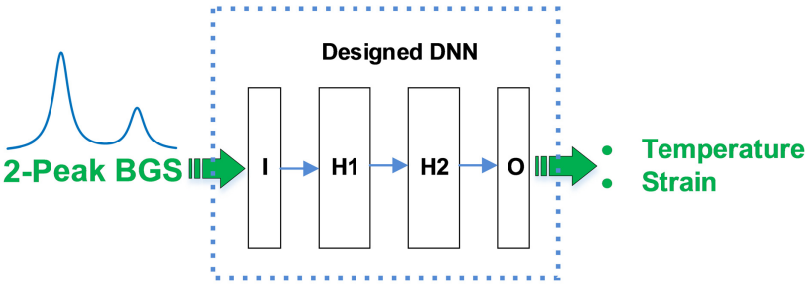

Fig. 2. Principle of using DNN for simultaneous temperature and strain measurement from double-peak BGS in LEAF. I: input layer; H1, H2: hidden layer; O: output layer.

We use theoretical double-peak Lorentzian BGS expressed in Eq. (2) to train the DNN,

$$g(\upsilon)=\frac{g_B^{Peak1}}{1+[(\upsilon-\upsilon_B^{Peak1})/(\Delta\upsilon_B^{Peak1}/2)]^2}+\frac{g_B^{Peak2}}{1+[(\upsilon-\upsilon_B^{Peak2})/(\Delta\upsilon_B^{Peak2}/2)]^2} \quad (2)$$

where $g(\upsilon)$ represents the normalized BGS, υ is the frequency difference between the probe and pump light in BOTDA, g_B^{Peak1} and g_B^{Peak2} are peak gains, υ_B^{Peak1} and υ_B^{Peak2} are BFSs, and $\Delta\upsilon_B^{Peak1}$ and $\Delta\upsilon_B^{Peak2}$ are Brillouin gain bandwidths for Peak 1 and Peak 2, respectively. In our case, the range of υ is from 10.550GHz to 11.000GHz with 2MHz interval, which is the same as the frequency scanning range during the acquisition of BGSs in experiment. g_B^{Peak1} is set to be 1 and g_B^{Peak2} varies to traverse all the values from 0.13 to 0.53 with 0.10 interval. This setting is consistent with the ratio between the 1st and 2nd Brillouin peak gains of our LEAF sensing fiber, which is pre-calibrated under different temperature and strain conditions used in the experiment. As a proof-of-concept demonstration, the temperature range in the training is from 40°C to 62°C with 2°C interval and the strain range is from 0με to 1860με with 60με interval, both of which can be further enlarged although more time for DNN training will be consumed. Note that to make the results more generalized, the values of the temperature and strain in the testing stage will be random which include those that do not appear in the training stage, e.g. 61°C and 1677.6με in our experiment. The two BFSs, i.e. υ_B^{Peak1} and υ_B^{Peak2}, of the ideal double-peak BGS are determined by using pre-calibrated BFS-temperature/strain coefficients of our LEAF sensing fiber. In order to accommodate BGS linewidth variations along the fiber [22], the range of $\Delta\upsilon_B^{Peak1}$ is from 46MHz to 66MHz with 2MHz interval and $\Delta\upsilon_B^{Peak2}$ is from 40MHz to 80MHz with 4MHz interval, so 11 pairs of $\Delta\upsilon_B^{Peak1}$ and $\Delta\upsilon_B^{Peak2}$ values are formed for the training. The above parameter setting to obtain the ideal BGSs for training is based on the pre-calibrated double-peak BGS of our LEAF sensing fiber and depends on the optimization process of DNN model through repeated trials for optimal performance. After training, the DNN model can be used to extract the temperature and strain values from the input BGS data directly. Since no procedure of solving two BFS equations is needed, the small matrix determinant induced large error can be avoided and the accuracy would be expected to improve. As there is no time-consuming curve fitting process to obtain the BFSs of the Brillouin peaks, the whole process of both temperature and strain extraction by DNN will be very fast. In the next section, we also describe the conventional equations solving method for comparison.

Optics EXPRESS

2.2 Conventional equations solving method for simultaneous temperature and strain measurement

It is known that the BFSs of Peak 1 and Peak 2 in LEAF sensing fiber have linear relationships with both temperature and strain, which are shown as Eqs. (3)–(4) [16–18,20],

$$\Delta BFS^{Peak1} = C_T^{Peak1} \cdot \Delta T + C_\varepsilon^{Peak1} \cdot \Delta\varepsilon \tag{3}$$

$$\Delta BFS^{Peak2} = C_T^{Peak2} \cdot \Delta T + C_\varepsilon^{Peak2} \cdot \Delta\varepsilon \tag{4}$$

where ΔBFS^{Peak1} and ΔBFS^{Peak2} are the BFS change of Peak 1 and Peak 2 under the temperature and strain change of ΔT and $\Delta\varepsilon$, respectively. C_T^{Peak1} and C_ε^{Peak1} are the BFS-temperature and strain coefficients for Peak 1, while C_T^{Peak2} and C_ε^{Peak2} are coefficients for Peak 2, respectively. In the conventional equations solving method [16–21], ΔBFS^{Peak1} and ΔBFS^{Peak2} are obtained by Lorentzian curve fitting (LCF) based on Eq. (2), and then the temperature and strain are obtained by solving Eqs. (3)–(4) as following [16–18,20],

$$\Delta T = \frac{C_\varepsilon^{Peak2} \cdot \Delta BFS^{Peak1} - C_\varepsilon^{Peak1} \cdot \Delta BFS^{Peak2}}{C_T^{Peak1} \cdot C_\varepsilon^{Peak2} - C_T^{Peak2} \cdot C_\varepsilon^{Peak1}} \tag{5}$$

$$\Delta\varepsilon = \frac{C_T^{Peak2} \cdot \Delta BFS^{Peak1} - C_T^{Peak1} \cdot \Delta BFS^{Peak2}}{C_T^{Peak2} \cdot C_\varepsilon^{Peak1} - C_T^{Peak1} \cdot C_\varepsilon^{Peak2}} \tag{6}$$

This is generally the procedure of the equations solving method to simultaneously measure the temperature and strain based on two BFSs of multi-peak BGS. However, as mentioned in [18,19], since the matrix determinant $C_T^{Peak1} \cdot C_\varepsilon^{Peak2} - C_T^{Peak2} \cdot C_\varepsilon^{Peak1}$ is usually very small, larger error will be produced when solving Eqs. (3)–(4) to obtain the temperature and strain, compared with the case of single temperature or strain measurement. Thus except the time-consuming curve fitting procedure, the equations solving method imposes stringent requirement on the resolution of BFS measurement, and is difficult to obtain the temperature and strain with high accuracy, especially when the FUT is long (e.g. several tens of kilometers) and the BFS resolution becomes worse.

2.3 Simulation results

Based on the parameter setting in Section 2.1, there are 12 temperature conditions, 32 strain conditions, 11 BGS linewidth conditions, and 5 peak gain conditions of Peak 2. Thus we have 12 × 32 × 11 × 5 = 21120 ideal double-peak Lorentzian BGSs and 12 × 32 = 384 target temperature and strain values in total for the DNN training. The DNN is trained using error back-propagation (BP) algorithm. After repeated trials with different number of hidden layers and neurons for optimal performance, the DNN model is eventually designed to have two hidden layers with 40 and 8 neurons, respectively. Two hidden layers are found to be enough for acceptable results, while more hidden layers will take much longer time for training but without obvious performance improvement. The following simulation and experiment results are all obtained using this DNN structure (226-40-8-2).

In this section, we first conduct simulation using simulated double-peak BGSs in the testing stage to evaluate the performance of DNN for simultaneous temperature and strain measurement. In the simulation, noisy BGSs are simulated by adding Gaussian white noise to the profile based on Eq. (2), and the signal-to-noise ratio (SNR) of the simulated BGSs is controlled by the amount of noise added. Note that the SNR of the simulated BGS is calculated by using the ratio between the amplitude of BGS peak and the standard deviation of its spectral points [27]. To improve the noise tolerance of the DNN model, we train the

Optics EXPRESS

DNN by using combined clean and noisy BGSs. The number of clean BGSs for training is 21120. The noisy BGSs with an SNR of 10.5dB for training are obtained by adding Gaussian white noise to the clean ones. Thus the total number of BGSs used for training is 42240. 10.5dB SNR is chosen since it just covers the lowest SNR level in our experiment, and the DNN trained with noisy BGSs of 10.5dB SNR is found to be enough to achieve the optimal performance for temperature and strain extraction in the experiment. After training, the DNN model is applied to extract both the temperature and strain from 1000 simulated testing BGSs of 20dB SNR, i.e. the case for low noise level. We have randomly selected five groups of target temperature and strain for the demonstration (40°C/50με; 45°C/200με; 52°C/1400με; 55°C/1600με; 60°C/1800με). As an example, we show the results for three groups of target temperature and strain in Fig. 3, which plots the extracted temperature and strain distribution by DNN. Fluctuations of the extracted temperature and strain are small, and the extracted values are close to the target ones for all the three cases. The detailed error performance of DNN is analyzed by calculating the Standard Deviation (SD) and Root Mean Square Error (RMSE) of the extracted temperature and strain, which is given in Table 1 for all five groups of target temperature and strain conditions. SD means the uncertainty or fluctuation of the extracted values; while RMSE indicates how close the extracted temperature and strain values are to the target ones, which is calculated by comparing the target values and extracted ones by DNN. The maximum SD and RMSE of the extracted temperature are only 0.5°C and 1.2°C, respectively; while those of the extracted strain are 13.5με and 43.7με, respectively. The results show that the DNN model trained by using combined clean and noisy BGSs performs well when extracting the temperature and strain from noisy testing BGSs with low noise level.

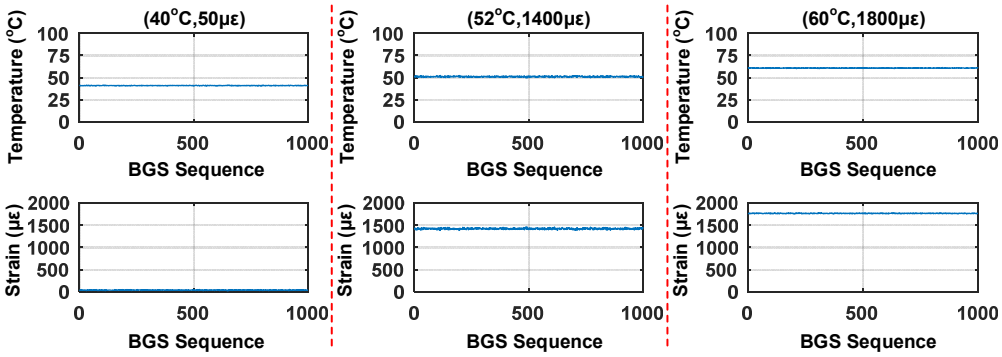

Fig. 3. Temperature and strain distribution extracted by DNN from 1000 simulated testing BGSs of 20dB SNR.

Table 1. Corresponding error performance of DNN for results in Fig. 3

Temperature (°C)	Strain (με)	Temperature (°C)		Strain (με)	
		SD	RMSE	SD	RMSE
40.0	**50.0**	0.2	1.2	4.9	11.7
45.0	**200.0**	0.4	1.1	9.2	43.7
52.0	**1400.0**	0.5	0.9	13.5	25.9
55.0	**1600.0**	0.3	0.8	8.9	14.3
60.0	**1800.0**	0.2	0.8	4.5	33.8

Next we further increase the noise level in the testing BGSs, and investigate the DNN performance. The DNN model is the same as that used in Fig. 3. Figure 4 shows the extracted temperature and strain distribution from 1000 simulated testing BGSs of 10.58dB SNR, which is the lowest SNR level observed in our experiment. Due to larger noise in the testing BGSs, the fluctuations of the extracted temperature and strain become a little larger than

Optics EXPRESS

those in Fig. 3, but the extracted values are still close to the target ones. For comparison, we also use the conventional equations solving method described in Section 2.2 to extract the temperature and strain from the same testing BGSs, and the results are given in Fig. 5. Note that we adopt Levenberg-Marquardt algorithm (LMA) for LCF to extract BFS [23], where it starts with an initial guess for the gain parameter, central frequency parameter and linewidth parameter, and then all of them are iteratively updated until the squared error converges. Besides large fluctuations, the extracted temperature and strain in Fig. 5 are far away from the target ones, and some extracted values are even out of the scales in Fig. 5, showing poor accuracy of the equations solving method when the noise is relatively high. As mentioned in Section 2.2, the low accuracy originates from the small difference in BFS coefficients between the two peaks, which gives rise to large error when solving the two BFS Eqs. (3)–(4). The detailed error performance for the results in Fig. 4 and Fig. 5 are compared in Table 2, which also includes the results for the other two groups of target temperature and strain. Take the target temperature and strain of (52.0°C, 1400.0με) as an example. The RMSE of the extracted temperature/strain by using DNN are 3.4°C/95.4με, while those by using the equations solving method are found to be 27.4°C/746.2με, respectively, which indicates that the errors of extracted temperature and strain by the equations solving method are about 8 times larger than those obtained by DNN. In all the five groups of target temperature and strain, the maximum SD of the extracted temperature/strain by DNN are 3.3°C/93.5με, and the maximum RMSE are 3.4°C/ 95.4με, respectively. While for the equations solving method, the maximum SD are 31.2°C/ 849.8με, and maximum RMSE are 31.2°C/852.0με, respectively. Although the error performance of DNN degrades a little due to larger noise in input testing BGSs, it still has significant improvement compared to that of the equations solving method.

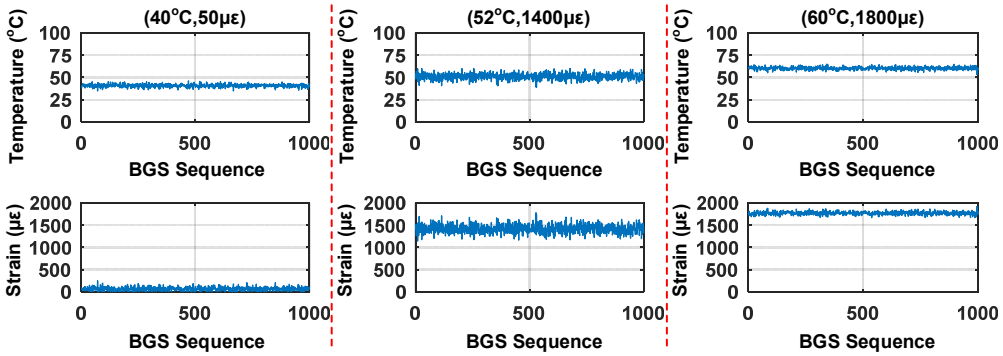

Fig. 4. Temperature and strain distribution extracted by DNN from 1000 simulated testing BGSs of 10.58dB SNR.

Optics EXPRESS

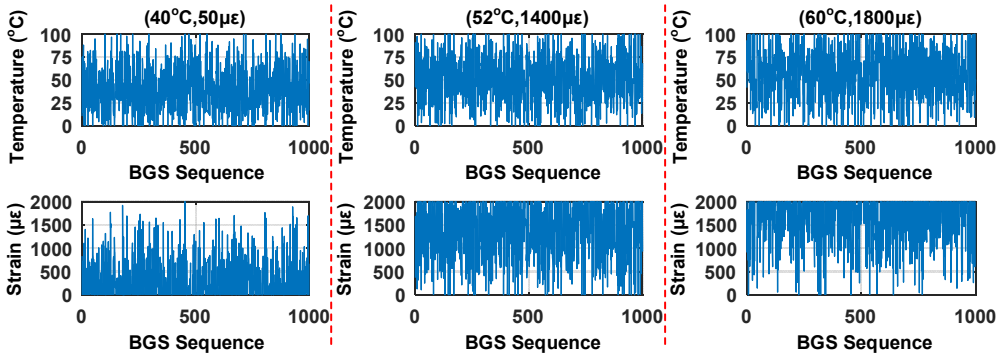

Fig. 5. Temperature and strain distribution extracted by the equations solving method from 1000 simulated testing BGSs of 10.58dB SNR.

Table 2. Corresponding error performance of DNN and the equations solving method for results in Figs. 4 and 5

Temperature (°C)	Strain (με)	Temperature (°C)				Strain (με)			
		DNN		Equations solving method		DNN		Equations solving method	
		SD	RMSE	SD	RMSE	SD	RMSE	SD	RMSE
40.0	**50.0**	1.7	1.9	26.2	26.2	42.3	45.3	714.7	714.7
45.0	**200.0**	2.4	2.8	25.5	25.5	63.2	74.0	693.9	694.0
52.0	**1400.0**	3.3	3.4	27.4	27.4	93.5	95.4	745.9	746.2
55.0	**1600.0**	2.4	2.6	26.9	26.9	66.1	68.6	733.5	733.8
60.0	**1800.0**	1.6	1.7	31.2	31.2	35.7	46.6	849.8	852.0

3. Experiment and results

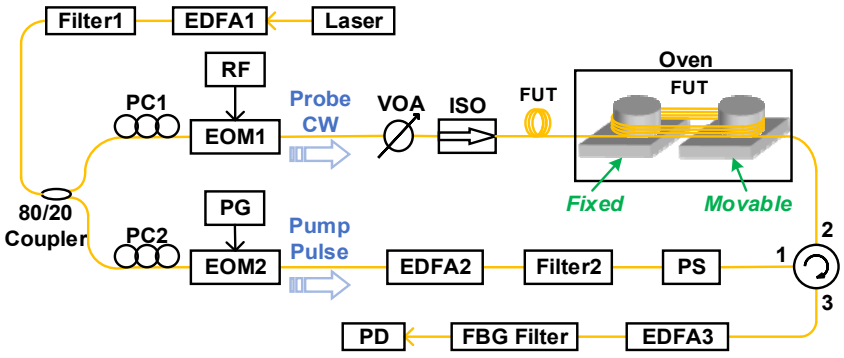

Fig. 6. BOTDA system setup. EDFA: erbium-doped fiber amplifier; PC: polarization controller; EOM: electro-optic modulator; RF: radio frequency; PG: pattern generator; VOA: variable optical attenuator; ISO: isolator; FUT: fiber under test; PS: polarization scrambler; FBG: fiber Bragg grating; PD: photodetector.

In this section, experimental BGSs under different real temperature and strain values are collected using the BOTDA setup shown in Fig. 6. The same DNN model as used in Fig. 3 and Fig. 4 is applied to extract both the temperature and strain distribution from experimental BGSs along the sensing fiber. In the BOTDA setup, the output of a continuous wave (CW) tunable laser working at 1550nm is amplified by an erbium-doped fiber amplifier (EDFA1) and is then split into two branches after filtering. The light at the upper branch is modulated

by an electro-optic modulator (EOM1) biased at null point to suppress the optical carrier and driven by a radio frequency (RF) signal generator to provide probe signal. A variable optical attenuator (VOA) is used to control the probe light power before it enters the fiber under test (FUT). At the lower branch, the CW light is modulated by the EOM2 to generate 20ns pump pulse. The EDFA2 is used to amplify the peak power of the pump pulse and the filter 2 is used to remove the amplified spontaneous emission (ASE) noise. The peak power of the pump pulse is 20dBm and the probe power is −8dBm, respectively. In addition, a polarization scrambler (PS) is used to suppress the polarization dependent noise. After passing through the FUT, the probe signal is amplified by EDFA3 and filtered to remove the higher frequency sideband. Finally, it is detected by a 125 MHz photodetector and collected on an oscilloscope. The FUT is a 24km long LEAF (Corning LEAF Optical Fiber ITU-T G.655.C), with its last 7m section heated (i.e. FUT inside the oven in Fig. 6) and the remaining section kept under room temperature and zero strain (i.e. FUT outside the oven in Fig. 6). And the 7m long FUT inside the oven is coiled on two micro-positioners, with one fixed and the other movable for applying different levels of uniform strain. Thus different temperature and strain conditions are applied to the 7m long FUT inside the oven. In order to have sufficient data points collected along the last 7m long FUT for the purpose of statistical analysis of the error performance, a relatively high sampling rate of 2.5GSample/s is adopted.

Figure 7(a) shows the measured BGS distribution along LEAF sensing fiber and Fig. 7(b) gives the measured double-peak BGS at one location of last 7m section when the temperature is 23.5°C and strain is 0με. The BFS-temperature relations and BFS-strain relations for BGS Peak 1 and Peak 2 are shown in Fig. 7(c) and 7(d), respectively. The BFS-temperature coefficients of Peak 1 and Peak 2 are measured to be 1.0546MHz/°C and 0.9380MHz/°C, respectively. While BFS-strain coefficients of the two peaks are measured to be 0.0385MHz/με and 0.0384MHz/με, respectively. As mentioned in Section 2.1, the coefficients and relations of BFS with temperature and strain are used to obtain ideal BGSs based on Eq. (2) for DNN training.

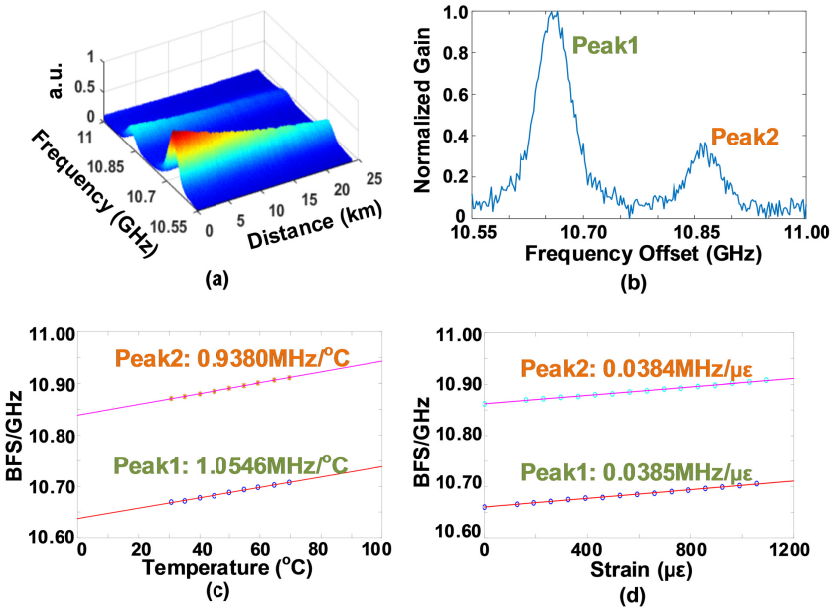

Fig. 7. (a) Measured BGS distribution along LEAF sensing fiber ; (b) measured double-peak BGS of LEAF under room temperature of 23.5°C and strain of 0με; (c) measured BFS-temperature relations for Peak 1 and Peak 2; (d) measured BFS-strain relations for Peak 1 and Peak 2.

Optics EXPRESS

In the experiment, we apply different values of temperature and strain to the last 7m FUT and collect the corresponding experimental BGSs which serve as the input testing BGSs to the DNN model for temperature and strain measurement. Eight groups of real temperature and strain conditions are randomly selected for the demonstration, which include values that do not appear in the training stage, e.g. (61°C, 1861.7με). As an example, we show the results for four groups of real temperature and strain conditions in Fig. 8. The blue curves in Fig. 8 show the temperature and strain distribution along the central part (4.7m section with relatively uniform strain) of the last 7m FUT extracted by using DNN. For comparison, the results by using the equations solving method are also given, shown as the orange curves in Fig. 8. It is obvious that the fluctuations of measured temperature and strain by using DNN are small, indicating small uncertainty of the measured temperature and strain. In contrast, the fluctuations by using the equations solving method are much larger. In addition, the measured values by using DNN are close to the real temperature and strain values, while those by using the equations solving method greatly deviate from the real values, e.g. the group of (56.0°C, 1660.8με) in Fig. 8. This means that the equations solving method has worse error performance, which agrees well with that in [18].

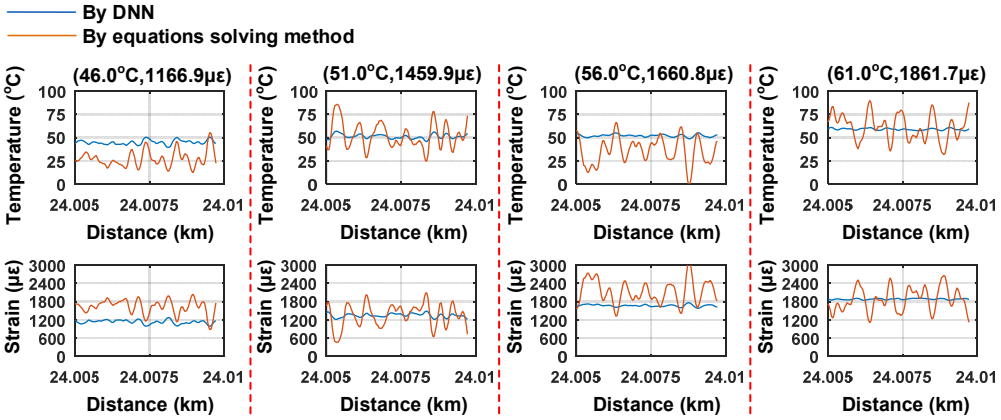

Fig. 8. Temperature and strain distribution along the central part of the last 7m FUT extracted by DNN (blue curve) and the equations solving method (orange curve), respectively.

Table 3. Corresponding error performance of DNN and the equations solving method for results in Fig. 8

Temperature (°C)	Strain (με)	Temperature (°C)				Strain (με)			
		DNN		Equations solving method		DNN		Equations solving method	
		SD	RMSE	SD	RMSE	SD	RMSE	SD	RMSE
46.0	**1166.9**	2.4	2.6	8.8	20.6	63.7	76.1	237.1	517.3
46.0	**1351.0**	2.4	2.4	11.9	24.4	66.2	96.5	320.9	616.2
51.0	**1459.9**	2.3	2.3	13.9	13.9	63.3	134.2	378.0	394.3
51.0	**1551.9**	2.0	3.4	11.8	15.1	59.5	90.2	322.9	356.9
56.0	**1660.8**	1.4	4.2	14.3	24.9	36.0	36.0	385.9	603.4
56.0	**1752.9**	1.3	3.1	14.3	30.1	26.8	65.7	383.2	710.2
61.0	**1677.6**	1.3	4.2	19.4	19.6	35.6	38.9	529.1	527.1
61.0	**1861.7**	1.0	2.3	14.1	14.1	18.8	26.2	383.2	381.6

The detailed comparison between the error performance using DNN and that using the equations solving method has been given in Table 3 for all the eight groups of real temperature and strain conditions. Similar to the simulation, SD and RMSE of the measured temperature and strain are calculated to evaluate the error performance of the experimental

results. The SD indicates the fluctuation of the measured temperature and strain, while the RMSE reflects how close the measured values are to the real ones. The real temperature values are read from a reference thermometer and the real strain values are obtained from the reading of the micro-positioner during the experiment. Since the strain along the central 4.7m section of the last 7m FUT is relatively uniform, the SD and RMSE are calculated using the data points along this section (117 data points in total under a sampling rate of 2.5GSample/s). From Table 3, we can see that in each group of temperature and strain, both the RMSE and SD by using DNN are much lower than those by using the equations solving method. Taking the group of (51.0°C, 1551.9.0με) as an example, the RMSE and SD of the measured temperature/strain by DNN are 3.4°C/90.2με and 2.0°C/59.5με, respectively; while the RMSE and SD by the equations solving method are found to be 15.1°C/356.9με and 11.8°C/322.9με, respectively. The errors of the measured temperature and strain by the equations solving method are more than four times larger than those by DNN. For DNN the worst RMSE of the measured temperature/strain in Table 3 are 4.2°C/134.2με, and the worst SD are 2.4°C/66.2με, respectively. While for the equations solving method, the worst RMSE are 30.1°C/710.2με, and worst SD are 19.4°C/529.1με, respectively. Much lower RMSE by DNN indicates that the measured temperature and strain values are closer to the real values, and lower SD by DNN implies that the fluctuations of the measured values are much smaller, as shown in Fig. 8. Thus compared with the equations solving method, DNN for simultaneous temperature and strain measurement has significantly improved the measurement accuracy. Moreover, since there are 600,000 BGSs along 24km LEAF at 2.5GSample/s sampling rate, the equations solving method with time-consuming LCF process takes 5656.3s to extract both the temperature and strain distribution from such large number of sensing points (computer platform: i7-6700K CPU and 16G RAM). While the DNN only consumes 1.6s for the same purpose, showing very fast processing speed for simultaneous temperature and strain measurement.

Besides the above situations with constant temperature and strain along the FUT inside the oven, we also implement the experiment in which abrupt changes of the environment occur along the FUT. The experiment setup is the same as that in Fig. 6, except the FUT inside the oven now has a length of 45m and is divided into three sections (i.e. Section 1 of 19m, Section 2 of 7m, Section 3 of 19m), with the strain only applied to the middle Section 2. As an example for the demonstration, we set the temperature of the oven to be 46.0°C and the applied strain to be 1166.9με. We compare the performance of the same DNN model and the equations solving method as used before, which are shown in Fig. 9 and Table 4. Similarly, we can see that the fluctuations of measured temperature and strain by using DNN are small, while those by using the equations solving method are much larger. And both the RMSE and SD by using DNN are much lower than those by using the equations solving method, as given in Table 4 for each section of FUT, implying better error performance of DNN when compared with the equations solving method.

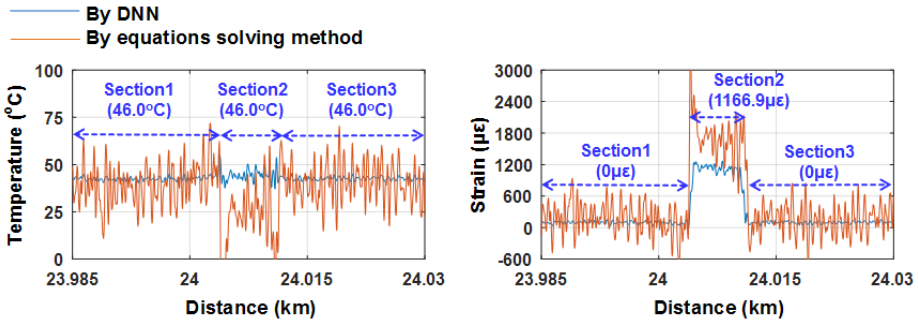

Fig. 9. Temperature and strain distribution along the FUT inside the oven extracted by DNN (blue curve) and the equations solving method (orange curve), respectively.

Optics EXPRESS

Table 4. Corresponding error performance of DNN and the equations solving method for results in Fig. 9

Fiber section	Temperature (°C)				Strain (με)			
	DNN		Equations solving method		DNN		Equations solving method	
	SD	RMSE	SD	RMSE	SD	RMSE	SD	RMSE
1	0.9	3.5	10.8	12.6	23.6	97.0	292.0	339.5
2	2.4	2.6	8.7	20.6	63.7	76.1	237.1	517.3
3	0.9	3.4	10.0	11.5	22.4	99.8	272.3	315.7

In our experiment, the total length of the FUT is 24km and our spatial resolution is 2m. The worst uncertainty of measured temperature and strain by the equations solving method is 19.4°C/529.1με, and they are improved to be 2.4°C/66.2με by using DNN. Note that Ref [18]. reports temperature and strain errors of 27°C/570με by the equations solving method for 22km LEAF length. Other works by the equations solving method demonstrate better error performance but within much shorter sensing distance, e.g. 3.9°C/83με in 2m PCF with spatial resolution of 15cm [16], 5°C/60με in 3.7km LEAF with spatial resolution of 2m [17], 1.8°C/37με in 377m LEAF with spatial resolution of 4m [19], 2.6°C/64.6με in 1km DCF with spatial resolution of 2m [20], and 1.2°C/21.9με in 3km few-mode fiber with spatial resolution of 2.5m [21]. And in [28] ANN has been used to classify the effect of temperature and strain in a standard single mode fiber (SSMF), but without the capability of measuring exact temperature and strain values, and no analysis of measured temperature and strain errors is given. Therefore, compared to the results in literature with similar sensing distance, our DNN approach shows much better accuracy than the equations solving method.

It is worth mentioning that in this work DNN extracts both the temperature and strain mainly from the two BFSs of double-peak BGS in LEAF, but it can also be applied to replace all the equations solving methods where any two of the parameters (e.g. BFS, Brillouin peak power, bandwidth, birefringence etc) are measured to build up the equations [12–21]. The large error induced by the small matrix determinant during the equations solving can be avoided and the accuracy would be improved. Moreover, multiple measured parameters can be potentially combined together as the input to the DNN model to further improve the accuracy of simultaneous temperature and strain measurement.

4. Conclusion

We have demonstrated simultaneous temperature and strain measurement by DNN assisted BOTDA system along 24km LEAF sensing fiber with a spatial resolution of 2m. DNN is trained by using combined ideal clean and noisy BGSs, and then extracts both the temperature and strain directly from the measured double-peak BGS with high accuracy. Both simulation and experiment under different temperature and strain conditions have been conducted to evaluate the DNN based temperature and strain measurement, with comparison to the conventional the equations solving method in terms of measurement accuracy and processing speed. Without the procedure of solving two BFS equations, the DNN scheme avoids the large error induced by the small matrix determinant, and hence greatly improves the measurement accuracy. The worst temperature/strain RMSE using DNN are 4.2°C/134.2με, much lower than that of 30.1°C/710.2με using the equations solving method; and the worst temperature/strain uncertainty using DNN are 2.4°C/66.2με, much smaller than that of 19.4°C/529.1με using the equations solving method, respectively. On the other hand, with no curve fitting process, the extraction of both temperature and strain by DNN becomes very fast. Only 1.6s is consumed by DNN to extract both the temperature and strain from 600,000 BGSs along 24km LEAF, which is much shorter than that of 5656.3s by the conventional equations solving method. We believe that the enhanced accuracy and fast processing speed make DNN a practical way of achieving simultaneous temperature and stain measurement in a single BOTDA system.

Optics EXPRESS

Funding

Hong Kong Polytechnic University (G-YBPH, 1-ZVHA); Project of Strategic Importance (1-ZVGB); Research Grants Council, University Grants Committee (RGC) (PolyU 5208/13E, 15265816, 15216817); National Natural Science Foundation of China (NSFC) (61377093, 61435006, U1701661).

References

1. A. Barrias, J. R. Casas, and S. Villalba, "A review of distributed optical fiber sensors for civil engineering applications," Sensors (Basel) **16**(5), 748 (2016).
2. C. Hong, Y. Zhang, G. Li, M. Zhang, and Z. Liu, "Recent progress of using Brillouin distributed fiber optic sensors for geotechnical health monitoring," Sens. Actuators A Phys. **258**, 131–145 (2017).
3. M. Soto, X. Angulo-Vinuesa, S. Martin-Lopez, S. Chin, J. Ania-Castanon, P. Corredera, E. Rochat, M. Gonzalez-Herraez, and L. Thevenaz, "Extending the real remoteness of long-range Brillouin optical time-domain fiber analyzers," J. Lightwave Technol. **32**(1), 152–162 (2014).
4. S. Diakaridia, Y. Pan, P. Xu, D. Zhou, B. Wang, L. Teng, Z. Lu, D. Ba, and Y. Dong, "Detecting cm-scale hot spot over 24-km-long single-mode fiber by using differential pulse pair BOTDA based on double-peak spectrum," Opt. Express **25**(15), 17727–17736 (2017).
5. X. H. Jia, H. Q. Chang, K. Lin, C. Xu, and J. G. Wu, "Frequency-comb-based BOTDA sensors for high-spatial-resolution/long-distance sensing," Opt. Express **25**(6), 6997–7007 (2017).
6. M. A. Soto and L. Thévenaz, "Modeling and evaluating the performance of Brillouin distributed optical fiber sensors," Opt. Express **21**(25), 31347–31366 (2013).
7. D. Zhou, Y. Dong, B. Wang, T. Jiang, D. Ba, P. Xu, H. Zhang, Z. Lu, and H. Li, "Slope-assisted BOTDA based on vector SBS and frequency-agile technique for wide-strain-range dynamic measurements," Opt. Express **25**(3), 1889–1902 (2017).
8. X. Bao and L. Chen, "Recent progress in Brillouin scattering based fiber sensors," Sensors (Basel) **11**(4), 4152–4187 (2011).
9. K. Kishida, Y. Yamauchi, and A. Guzik, "Study of Optical Fibers Strain-Temperature Sensitivities Using Hybrid Brillouin-Rayleigh System," Photonic Sens. **4**(1), 1–11 (2014).
10. M. N. Alahbabi, Y. T. Cho, and T. P. Newson, "Simultaneous temperature and strain measurement with combined spontaneous Raman and Brillouin scattering," Opt. Lett. **30**(11), 1276–1278 (2005).
11. Z. Zhao, Y. Dang, M. Tang, L. Duan, M. Wang, H. Wu, S. Fu, W. Tong, P. P. Shum, and D. Liu, "Spatial-division multiplexed hybrid Raman and Brillouin optical time-domain reflectometry based on multi-core fiber," Opt. Express **24**(22), 25111–25118 (2016).
12. X. Bao, Q. Yu, and L. Chen, "Simultaneous strain and temperature measurements with polarization-maintaining fibers and their error analysis by use of a distributed Brillouin loss system," Opt. Lett. **29**(12), 1342–1344 (2004).
13. W. Zou, Z. He, and K. Hotate, "Complete discrimination of strain and temperature using Brillouin frequency shift and birefringence in a polarization-maintaining fiber," Opt. Express **17**(3), 1248–1255 (2009).
14. Y. Dong, L. Chen, and X. Bao, "High-spatial-resolution simultaneous strain and temperature sensor using Brillouin scattering and birefringence in a polarization-maintaining fibre," IEEE Photonics Technol. Lett. **22**(18), 1364–1366 (2010).
15. Z. Zhao, Y. Dang, M. Tang, B. Li, L. Gan, S. Fu, H. Wei, W. Tong, P. Shum, and D. Liu, "Spatial-division multiplexed Brillouin distributed sensing based on a heterogeneous multicore fiber," Opt. Lett. **42**(1), 171–174 (2017).
16. L. Zou, X. Bao, S. Afshar V, and L. Chen, "Dependence of the brillouin frequency shift on strain and temperature in a photonic crystal fiber," Opt. Lett. **29**(13), 1485–1487 (2004).
17. C. C. Lee, P. W. Chiang, and S. Chi, "Utilization of a dispersion-shifted fiber for simultaneous measurement of distributed strain and temperature through Brillouin frequency shift," IEEE Photonics Technol. Lett. **13**(10), 1094–1096 (2001).
18. M. Alahbabi, Y. T. Cho, and T. P. Newson, "Comparison of the methods for discriminating temperature and strain in spontaneous Brillouin-based distributed sensors," Opt. Lett. **29**(1), 26–28 (2004).
19. X. Liu and X. Bao, "Brillouin spectrum in LEAF and simultaneous temperature and strain measurement," J. Lightwave Technol. **30**(8), 1053–1059 (2012).
20. Z. Li, L. Yan, X. Zhang, and W. Pan, "Temperature and Strain Discrimination in BOTDA Fiber Sensor by Utilizing Dispersion Compensating Fiber," IEEE Sens. J. **18**(17), 7100–7105 (2018).
21. A. Li, Y. Wang, J. Fang, M. J. Li, B. Y. Kim, and W. Shieh, "Few-mode fiber multi-parameter sensor with distributed temperature and strain discrimination," Opt. Lett. **40**(7), 1488–1491 (2015).
22. A. K. Azad, L. Wang, N. Guo, H. Y. Tam, and C. Lu, "Signal processing using artificial neural network for BOTDA sensor system," Opt. Express **24**(6), 6769–6782 (2016).
23. H. Wu, L. Wang, N. Guo, C. Shu, and C. Lu, "Brillouin optical time domain analyzer assisted by support vector machine for ultrafast temperature extraction," J. Lightwave Technol. **35**(19), 4159–4167 (2017).

Optics EXPRESS

24. H. Wu, L. Wang, N. Guo, C. Shu, and C. Lu, "Support vector machine assisted BOTDA utilizing combined Brillouin gain and phase information for enhanced sensing accuracy," Opt. Express **25**(25), 31210–31220 (2017).
25. B. Wang, N. Guo, F. N. Khan, A. K. Azad, L. Wang, C. Yu, and C. Lu, "Extraction of Temperature Distribution Using Deep Neural Networks for BOTDA Sensing System," in *2017 Conference on Lasers and Electro-Optics Pacific Rim (CLEO-PR)*, paper s2027.
26. B. Wang, L. Wang, C. Yu, and C. Lu, "Simultaneous temperature and strain measurement using deep neural networks for BOTDA sensing system," in *The Optical Fiber Communication Conference and Exhibition 2018 (OFC)*, paper Th2A.66, pp. 1–3.
27. A. Lopez-Gil, M. A. Soto, X. Angulo-Vinuesa, A. Dominguez-Lopez, S. Martin-Lopez, L. Thévenaz, and M. Gonzalez-Herraez, "Evaluation of the accuracy of BOTDA systems based on the phase spectral response," Opt. Express **24**(15), 17200–17214 (2016).
28. R. Ruiz-Lombera, A. Fuentes, L. Rodriguez-Cobo, J. M. Lopez-Higuera, and J. Mirapeix, "Simultaneous temperature and strain discrimination in a conventional BOTDA via artificial neural networks," J. Lightwave Technol. **36**(11), 2114–2121 (2018).